arXiv:0706.2639v1 [quant-ph] 18 Jun 2007

Apparatus for excitation and detection of Rydberg atoms in quantum gases

Robert Löw,* Ulrich Raitzsch, Rolf Heidemann, Vera Bendkowsky, Björn Butscher, Axel Grabowski, and Tilman Pfau

5. Physikalisches Institut, Universität Stuttgart, Germany

(Dated: February 1, 2008)

We present and characterize a versatile experimental setup which allows for excitation and detection of Rydberg atoms in quantum gases. The novel concept of the setup features two charged particle detectors and eight electrical field plates inside the vacuum chamber, which allows the detection and manipulation of Rydberg atoms. The setup presented here is applicable to all atomic species used in the field of quantum gases. We describe and characterize the production of Bose-Einstein condensates, the excitation scheme into Rydberg states, the detection of Rydberg states by field ionization followed by ion detection and the various electric field configurations provided by the eight field plates.

PACS numbers:

I. INTRODUCTION

Over the last two decades scientists have developed a huge variety of different vacuum chamber designs serving distinctive purposes for experiments in atom optics. An important and challenging task in many experiments is the reliable production of Bose-Einstein condensates (Cornell and Wieman, 2002; Ketterle, 2002) in combination with additional experimental tools. Depending on the physics to investigate specialized setups have been developed explore transportable condensates (Chikkatur *et al.*, 2002), toroidal shaped condensates (Gupta *et al.*, 2005), condensates on microchips (Fortagh *et al.*, 1998; Hänsel *et al.*, 2001). Other designs featuring experimental extensions like high finesse cavities (Ottl *et al.*, 2006) and multi-channel plates (Robert *et al.*, 2001) have been realized. Here, we present a new apparatus for the investigation of Rydberg atoms in ultracold quantum gases. The setup itself is based on a standard BEC-setup (Streed *et al.*, 2006), which is used in many atom optician laboratories over the world, though, it has the unique capability to investigate and manipulate Rydberg atoms in the quantum degenerate regime.

Bose-Einstein condensates are produced by trapping and cooling atoms from a thermal atom source, usually from a solid alkali metal. After slowing down the velocity of the thermal atoms by several orders of magnitude they can be trapped in a magneto-optical trap, that is, three pairs of laser beams confining the atoms around the center of a superposed magnetic quadrupole field. Due to scattering of light in the magneto-optical trap it is not possible to achieve condensation in this type of trap. Thus, the atoms have to be loaded in a trap, in which the confining potential is not build up by near resonant light.

One possibility to realize a conservative trapping potential is an intense far off resonant light field (FORT). The trapping potential is build up by the dipole force, which is due to the interaction between the light and the induced dipole moment of the atom. Another possibility, and by far the most common, is to trap the atoms magnetically in a Ioffe-Pritchard type trap (Ernst *et al.*, 1998). The Ioffe-Pritchard trap is formed by a radial 2D quadrupole field and an axial dipole field, which yields a radial gradient and a superposed axial curvature. Once the atoms are tightly confined evaporative cooling is applied to cool the atoms into the quantum degenerated regime in which the ground state is macroscopically occupied and the atoms form a coherent matter wave.

The combination of Bose-Einstein condensates with Rydberg atoms opens a new field of research aiming for strong interactions and strongly correlated mesoscopic systems. The coherence properties of quantum degenerate gases in combination with a coherent excitation scheme into Rydberg states yields an ideal tool box to study decoherence processes in mesoscopic systems (Heidemann *et al.*, 2007) and for testing the preconditions for quantum computing (DiVincenzo, 2000; Jaksch *et al.*, 2000). The strong interaction between Rydberg atoms is governed either by the van der Waals interaction, which can induce a blockade effect in Rydberg excitation (Heidemann *et al.*, 2007; Singer *et al.*, 2004a; Tong *et al.*, 2004) or the anisotropic dipole-dipole interaction. A handy feature of Rydberg atoms is the tunability of the interaction strength by either choosing a certain Rydberg state or by applying suitable electric fields (Gallagher, 1994).

Far reaching insight in the properties of Rydberg atoms have been achieved by experiments on thermal atomic beams (Koch, 1983). With the discovery of laser cooling techniques (Chu, 1998; Cohen-Tannoudji, 1998; Phillips, 1998) it is now possible to extend the experiments to so called frozen Rydberg gases

---

*Electronic address: r.loew@physik.uni-stuttgart.de

(Anderson *et al.*, 1998; Mourachko *et al.*, 1998). The name reflects the fact that the atomic motion at temperatures in the microkelvin regime are nearly frozen out during the typical experimental timescales of several microseconds. The relatively high densities of several 10^{16} atoms/m^3 privilege these systems to investigate the interaction among Rydberg atoms. In such systems several groups have investigated the van-der-Waals interaction (Amthor *et al.*, 2007; Farooqi *et al.*, 2003; Singer *et al.*, 2004b; Tong *et al.*, 2004) and the resonant dipole-dipole interaction (Afrousheh *et al.*, 2004; Anderson *et al.*, 1998; Vogt *et al.*, 2006) including the angular dependence of the dipole-dipole interaction (Carroll *et al.*, 2004). With the observation of a coherent excitation (Cubel *et al.*, 2005; Deiglmayr *et al.*, 2006) is it now possible to study the coherence properties of mesoscopic quantum systems under the influence of strong interactions (Heidemann *et al.*, 2007). Closely related to the frozen Rydberg gases is the simultaneously evolving research field on ultracold plasmas (Killian *et al.*, 1999; Robinson *et al.*, 2000), which can be studied in the same setups.

Finally, the extension of such setups to degenerate quantum gases increases not only the parameter space of available densities and temperatures by several orders of magnitude, but allows also for phase sensitive measurements using a coherent matter wave with well defined internal and external states.

Besides the ability of the apparatus to produce stable Bose-Einstein condensates working with ultracold Rydberg atoms requires a modification of the common setups. Especially components to apply strong electric fields over the atomic cloud and ion or electron detectors for the detection of Rydberg atoms are required. Additionally a narrow-band laser system is required, to excite the atoms into specific Rydberg states or to gain coherent control over the excitation.

This paper is organized in the following way. We describe the vacuum chamber in the next section, followed by a characterization of the Bose-Einstein condensate in section III. The sections IV and V are covering the manipulation of the Rydberg atoms, namely, introducing the Rydberg laser system and the electric field generation. The detection of Rydberg atoms is presented in section VI followed by a measurement of a Stark map in section VIII. In the end an outlook is given in section IX.

II. VACUUM SYSTEM

The vacuum chamber consists mainly of two parts as shown in Fig. 1. The oven assembly, which is operated at high vacuum (10^{-7} mbar), delivers a thermal beam of gaseous Rubidium atoms into the ultra-high vacuum part of the setup ($< 2 \cdot 10^{-11}$ mbar) for further processing. The basic design of our setup can be found in several experimental groups in similar realizations and a detailed description of its basic principles can be found in (Streed *et al.*, 2006). At the given pressure in the main chamber we measured a lifetime of more than 160 seconds of magnetically trapped ^{87}Rb atoms.

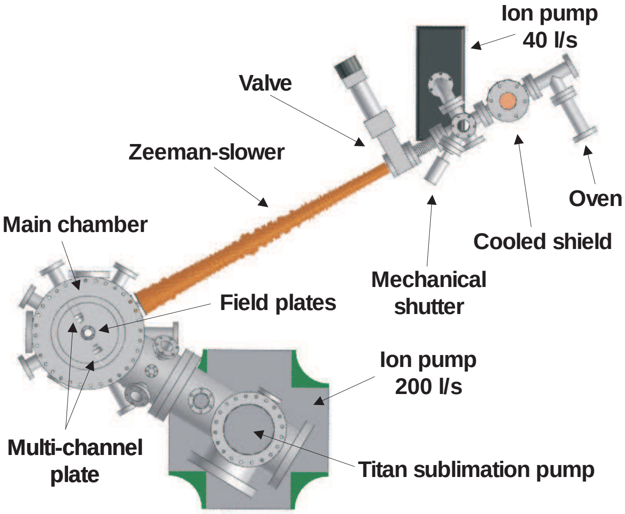

FIG. 1 Overview of the complete vacuum system. A thermal beam of Rb-atoms is produced with an effusive oven and slowed down with a Zeeman-slower which connects the oven part with the main chamber. The required ultra-high vacuum in the main chamber is accomplished with an ion pump and a titanium sublimation pump, which can be cooled down with liquid nitrogen.

The production of a Bose-Einstein condensate consists of several successive experimental steps. The starting point is a magneto-optical trap (MOT), which is in our case loaded by an atomic beam produced by an effusive oven and slowed down by a Zeeman-slower. Within a few seconds several 10^{10} atoms are caught in the MOT. To reduce the temperature of the magneto-optically trapped atoms to about 25-30 µK we apply a grey molasses cooling scheme for 30 ms (Lett *et al.*, 1989). As a next step the atoms are optically pumped to the $F = 2, m_F = 2$ state and transferred into a best possible mode-matched pure magnetic trap. In this trap the atomic cloud is cooled down within 30 s to quantum degeneracy by forced evaporative cooling using radio-frequency techniques. By this procedure we are able to produce Bose-Einstein condensates with $3 \cdot 10^5$ atoms every 40 s.

The main chamber depicted in Fig. 2 has to fulfill several boundary conditions simultaneously. First of all, good optical access in three dimensions for laser cooling is necessary. Two further optical axes are added for imaging which are equipped with two larger view-ports (CF 63) to obtain a better optical resolution. The numerical apertures in both imaging axes are 0.17 which yields an optimal resolution of 5.6 µm for a wavelength of 780 nm. Altogether eleven optical view-ports (7056 glass) are available which are suitable for wavelengths ranging from 300 nm to 2.5 µm. At the same time close by magnetic coils for magnetic trapping are necessary.

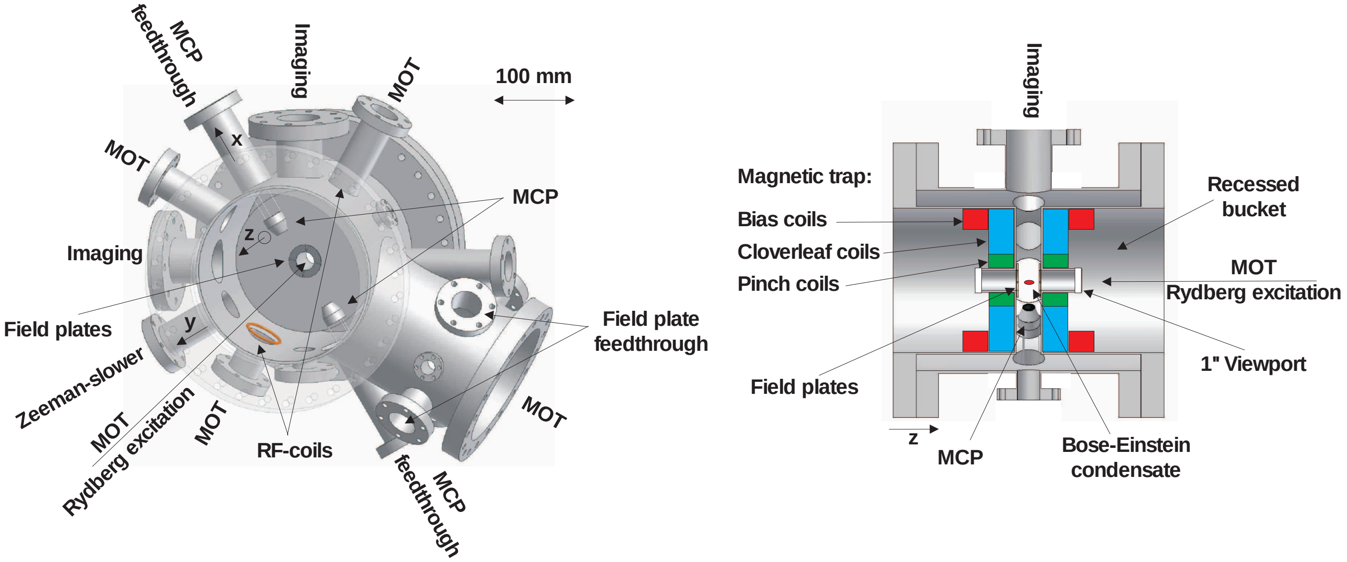

FIG. 2 Detailed view of the main chamber. In the left part of the figure is one recessed bucket removed to reveal the components used for electrical field manipulation and Rydberg atom detection. The right part of the figure shows a slice of the main chamber including both recessed buckets. Inside the buckets, but outside the vacuum, are the coils for magnetic trapping located. More details are given in the text.

We use a cloverleaf style Ioffe-Pritchard trap (Pritchard, 1983; Streed *et al.*, 2006) which is located inside two recessed bucket windows outside the vacuum. The inner spacing of the two coil assemblies is 32 mm. The two pinch coils of the cloverleaf trap produce an axial curvature of $B'' = 0.56$ G/cm^2 per Ampere and the leafs a radial gradient of $B' = 0.61$ G/cm per Ampere. At typical operation conditions with 400 A in all coils and an offset field of 1.5 G we obtain for ^{87}Rb trapped in the $F = 2, m_F = 2$ state trapping frequencies of 18 Hz axially and 250 Hz radially.

The main goal of the setup described here is the investigation of Rydberg atoms excited from Bose-Einstein condensates. For the manipulation and detection of the highly excited atoms we included eight field plates and two multi-channel plates (MCP) close to the atoms inside the vacuum. The details of this add-ons will be discussed in detail below. Because of the arrangement of the field plates we had to relocate the radio-frequency coils used for evaporative cooling further away from the atoms as can be seen in Fig. 2 and Fig. 5. We use two coils made of polyimid coated copper wires consisting each of two loops. Remanent charge on the insulating coating can cause disturbing electric fields if they are too close to the atoms, which is also avoided by the larger distance of the coils. Nevertheless, the coils produce at the position of the atoms an average magnetic field of 5 mG (for frequencies from 1 to 30 MHz), when driven with 2 W. This is sufficient to drive the magnetic dipole transitions for evaporative cooling.

III. BOSE-EINSTEIN CONDENSATION

Typically we perform evaporative cooling for 30 s on the magnetically trapped cloud until we reach the critical temperature T_c at roughly 400 nK for the given trap parameters. The analysis of the Bose condensed clouds is done after some time-of-flight with the absorption imaging technique. In Fig. 3 a purely thermal cloud at $T \approx T_c$ is shown and a cloud at $0.7 \cdot T_c$ with a condensate fraction of 65 %, both after a free expansion of 21 ms. The temperature of the cloud is obtained by fitting a Gaussian distribution to the wings (indicated by the vertical lines) of the recorded density distribution. The width of the Gaussian distribution determines then, with the knowledge of the free expansion time, the temperature of the cloud, assuming a point-like trapped cloud. Apparently the atomic cloud at $T = T_c$ is not Gaussian anymore. The Bose enhancement plays already above T_c a crucial role. The blue line is a fit to a Bose distribution where the chemical potential was set to zero. From this fit we deduce the atom number in the thermal cloud for all temperatures below T_c. In a next step we subtract the fitted Bose distribution from the data and assign the remaining part to the Bose-Einstein condensate. The density distribution in Thomas-Fermi approximation follows a parabolic shape for a harmonic trapping potential. With this it is now possible to extract the condensate fraction, which is the number of atoms in the condensed phase divided by the total atom number. With the knowledge of the condensed atom number and the trapping frequencies all important parameters of the atomic cloud are determined. A trapped BEC with $3 \cdot 10^5$ atoms has a radial Thomas-Fermi radius of 3.3 µm and an axially radius of

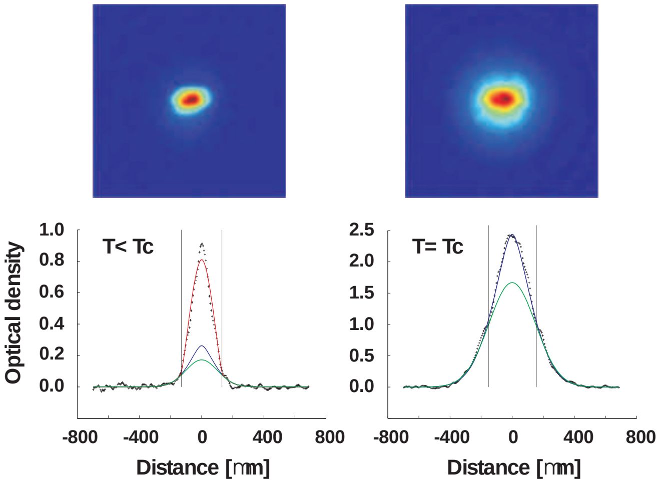

FIG. 3 Density distribution at different temperatures. The pictures show a central slice of two absorption images taken after 21 ms time of flight. The figure on the right is a thermal cloud just at the critical temperature. On the left an atomic cloud well below T_c is shown. The vertical black lines indicate the part of the clouds which was taken for fitting the thermal contribution. The green curve is a Gaussian fit on the wings beyond the black lines. The blue line is the Bose enhanced distribution, which shows that there is actually no condensate fraction present in the right figure. Finally the red line is the condensate fraction in Thomas-Fermi approximation.

46 µm. The peak density is $3.5 \cdot 10^{14}$ cm^{-3} and the corresponding chemical potential is roughly 3 kHz · in units of Plancks constant.

IV. LASERSYSTEM FOR RYDBERG EXCITATION

The excitation into Rydberg states with principal quantum numbers ranging from n=20 up to the ionization threshold is accomplished by a two-photon excitation scheme. For a single photon excitation one has to use light at 297 nm, which is difficult to produce. In the two-photon excitation scheme the first laser is tuned close to resonance to a transition of the ground state to an intermediate state, from which the second photon takes the atom to the desired Rydberg state. The polarizability of the intermediate state enhances the coupling of the ground state to the Rydberg state. By choosing a sufficient large detuning with respect to the intermediate state one avoids population of the intermediate state and one obtains effectively a two level system. In our case we use as an intermediate state the $5P_{3/2}$ state which corresponds to wavelengths at 780 nm and 480 nm. The red light (780 nm) is produced by a standard external cavity diode laser setup, whereas the blue light (480 nm) is generated by frequency doubling laser light of a tapered amplifier at 960 nm. Fig. 4 depicts the schematic setup of the laser system. The two laser systems for the red (780 nm) and the infrared (960 nm) light, as well all elements for frequency stabilization are located in a separate room to increase the stability. By this we reached an overall line-width of the two photon excitation of about 1.5 MHz for excitation times above one millisecond. On the timescale of our experiments of several microseconds we measure a line-width of about 130 kHz. The infrared light is brought to the laboratory by a polarization maintaining (PM) optical fiber, passes a tapered amplifier, a frequency doubling cavity (TA-SHG 110, Toptica Photonics AG, Germany) and is finally guided by another PM-fiber to the experiment. A third PM-fiber takes the light at 780 nm to the experiment.

Our setup allows us to choose easily different laser frequencies for manifold experimental situations. The frequency of the 780 nm light is stabilized with a standard polarization spectroscopy method (Demtröder, 2002) to any desired line or crossover of the $5S_{1/2} \rightarrow 5P_{3/2}$ transition manifold. Before it enters the vacuum chamber, it passes an acousto-optical modulator (AOM) in a double-pass configuration. With this AOM we can switch the light within 20 ns and tune the frequency of the light by 200 MHz within the 3dB bandwidth. In combination with the locking scheme we can tune the light right on any resonance, or detune it at most by 500 MHz with respect to any transition line of the $5S_{1/2} \rightarrow 5P_{3/2}$ manifold. The transfer cavity is used to stabilize the 960 nm light to the already stabilized 780 nm light (Bohlouli-Zanjani *et al.*, 2006). The 30 cm long cavity is made of stainless steel and has a mode spacing of 125 MHz. Its length can be altered by a piezo actuator, which is used to stabilize the length of the cavity onto the transmission signal of the 780 nm light. We evacuated the cavity to avoid changes in the refractive index of the air due to atmospheric pressure and humidity. The master laser at 960 nm can now be stabilized to any mode of the cavity in steps of 125 MHz. A subsequent AOM in double pass configuration allows us to scan the infrared light by 300 MHz, which corresponds to 600 MHz of the frequency doubled blue light at 480 nm. To scan a larger frequency region than available by the AOM, we control the grating of the infrared diode laser directly and scan by this the frequency without mode hops for more than 12 GHz in the blue light. To calibrate the frequency of the scanned region we simultaneously record the signal from the stabilized Fabry Perot resonator.

The two laser beams for the two-photon excitation are spatially overlapped before entering the vacuum chamber at a dichroic mirror. The overlapped beams were aligned parallel to the z-axis, which is also the quantization axis of the magnetic trap. The polarization of both beams was set to σ^+ respectively σ^- to maintain the magnetic moment of the atom and avoid frequency shifts due to magnetic fields. At the position of the atoms the 1/e^2 radius of the 780 nm light was set to 550 µm and the one at 480 nm to 35 µm. The maximum available laser power in the blue light (480 nm) is about 55 mW at the position of the atoms. In most experiments the power of the 780 nm light is reduced well below one milliwatt to

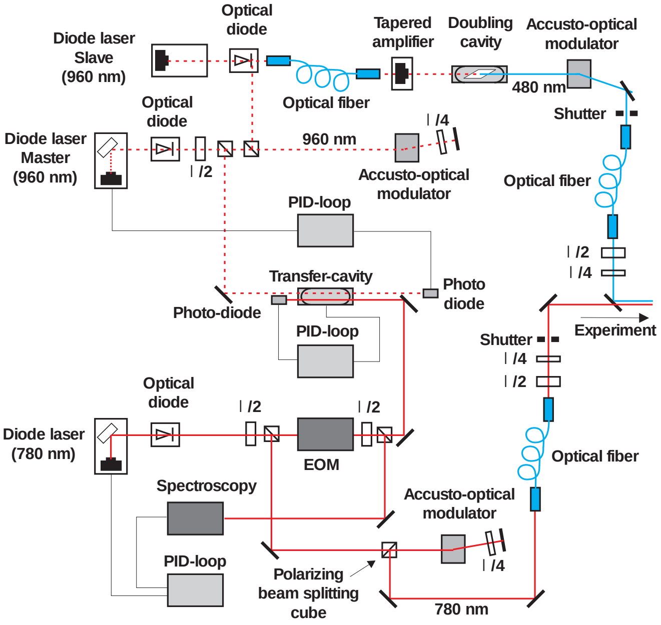

FIG. 4 Laser-system for two photon excitation of ^{87}Rb into Rydberg states. The red light at 780 nm is generated by a standard external cavity diode laser system. The production of blue light in the range of 475 nm to 483 nm is more involved. For this purpose we use a master slave setup, where a standard diode laser setup delivers infrared light at 960 nm which is amplified by a tapered amplifier. A subsequent frequency doubling cavity delivers the desired wavelength. After stabilizing a transfer cavity to the red light at 780 nm this cavity is used to stabilize the blue light at 480 nm with respect to the 780 nm light. The red light at 780 nm is locked to a spectroscopy signal produced in a Rubidium gas cell.

avoid excitation into the $5P_{3/2}$ state. At an detuning of 480 MHz (see Fig. 8) and a typical laser power of e.g. 50 µW the spontaneous scattering rate reduces to below one 1 kHz. The effective two photon Rabi frequency at this setting is 250 kHz. Another important aspect the uniformity of the illumination of the atoms. An atomic cloud at e.g. 3.4 µK confined in our magnetic trap at an offset field of 0.89 G, as used in (Heidemann *et al.*, 2007), has a Gaussian shape with a radial width of $\sigma_\rho = 8.6$ µm. At this parameters 85 % of the atoms experience at least 80 % of the maximum two photon Rabi frequency.

V. ELECTRIC FIELD PLATES

The high sensitivity of Rydberg atoms to electric fields opens the possibility to manipulate the internal states of the Rydberg atoms by field plates (MacAdam and Hwang, 2003). To produce electric field configurations as versatile as possible, we installed eight field plates close to the atoms. The spatial arrangement can be seen in Fig. 5 and Fig. 2. Each of these plates can be addressed individually, which allows us to generate nearly any field configuration starting from constant fields in arbitrary directions, to gradient fields, quadrupolar fields, hyperbolic concave saddles or hyperbolic convex fields with a positive curvature in all three dimensions. Some realizations are shown in Fig. 6.

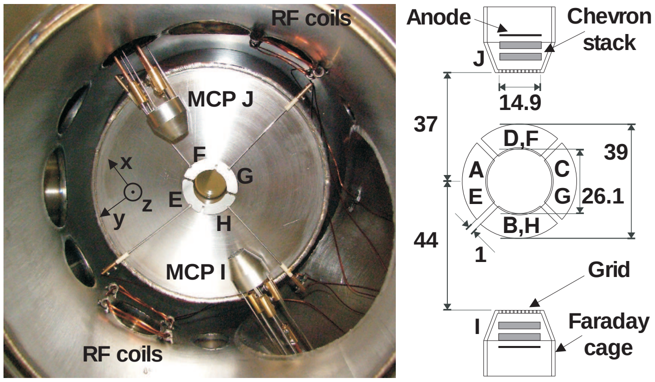

FIG. 5 Electric field plates (A-H) and Faraday cages (I and J) for the multi-channel plates. Four field plates are glued onto each of the resessed buckets, such that plate A, B, C, and D lie vis-a-vis to the plates E, F, G and H. The inner distance between the plates is 25 mm. All dimensions given in the figure are in millimeters. The MCPs were located as close as possible to the center of the vacuum chamber without loosing any optical access, which resulted in the two different distances.

The eight field plates are made of stainless steel with a thickness of 0.5 mm. They are glued with 1 mm thick ceramic spacers onto the resessed buckets. The dimensions of the spacers have to be small enough, that they are completely hidden behind the field plates from the viewpoint of the atoms. Any insulating surface can accumulate charge and falsify the desired field configuration. To charge the field plates they are spot welded to a stainless steel wire, which are radially led outwards as can be seen in Fig. 2. At the edge of the resessed bucket the wires are fixed in position by short ceramic tubings, which are also glued to the buckets and are subsequently connected to capton insulated copper wires. These copper wires are then finally connected to one of the fourfold high voltage feedthroughs. To avert breakthroughs inside the chamber induced by sharp edges we rounded off all four edges of each plate with a radius of 1.5 mm. Finally, we etched and electro-polished all field plates including the spot welded wires to burnish also small spikes. The polishing was done in a acid bath consisting of one part of 96% sulfuric acid, two parts of 85% phosphoric acid and six parts of distilled water. After two minutes at a current of 5 A about 70 µm of stainless steel from the plates was removed and they exhibited a semi gloss surface. After installation of the field plates and evacuating the chamber we measured no current leakage up to 3000 Volts for all plates.

During the experimental process it is necessary to switch the applied voltages within short times. To do so we use bipolar high voltage switches (HTS-6103 GSM, Behlke Electronic GmbH, Germany), which have an in-

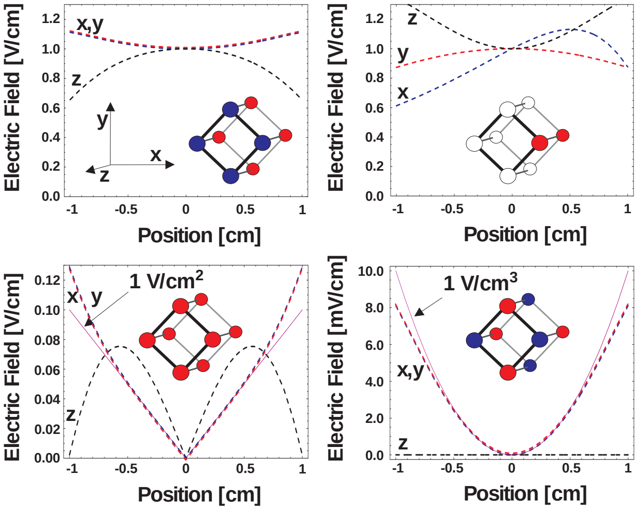

FIG. 6 Simulation of four different electric field configurations produced by an asymmetric octopole. The field plates are represented by point charges located at the corners of a cuboid with an aspect ratio of x:y:z=15:15:14 (mm). This simple geometry gives an excellent agreement with the electric fields of the real geometry, which have also been simulated by an elaborate finite element method. All four graphs show the absolute value of the calculated electric field along the coordinate axes as defined in Fig. 2 and Fig. 5. The upper left graph shows the realization of a preferably constant field by setting the charges A, B, C and D to a charge -Q (blue) and E, F, G and H accordingly to +Q (red). The upper right graph shows a simplified implementation of a constant electric field by setting charges B and H to +Q, which was used in our measurements in section VIII. On the lower left side is the realization of a gradient field along all three axes is shown (by setting all charges to the same value), which could be used in order to excite atoms space selective into Rydberg states. Finally the graph on the lower right shows an electric field distribution with a curvature in two directions, which is realized by charging the plates in an alternate pattern.

trinsic rise-time of 60 ns. The push-pull circuit of the switch has to be adjusted to match the capacitive load of 50 pF of each field plate as well the 300 pF load of the high voltage coax cable, which connects the switch to the high voltage feedthroughs.

The electric field distributions generated by the field plates and the Faraday cages of the MCPs have been calculated for several applications by finite element methods. This method is quite time consuming but gives good results for a given set of voltages applied to the 8 field plates and the two Faraday cages. But it is useless, when starting from a desired field distribution and asking for the required voltages. To do so, we use a simplified model consisting of point charges sitting at the corners of a cuboid. By expansion of the electric field into a Taylor series one can generate a set of linear equations, which can be used to calculate the voltages for a given electric field as shown in Fig. 6.

VI. DETECTION OF RYDBERG STATES

For a high detection sensitivity of Rydberg atoms, we installed two MCPs (Type B012VA, El-Mul Technologies Ltd, Israel) inside the vacuum chamber. After field ionization of the Rydberg atoms, we use one MCP to detect the ions. The second MCP is designated to detect simultaneously the electrons. To improve the amplification even further we use MCPs in a Chevron configuration, which consist of two successive glass plates with a small spacing in-between. The electron current arriving at the anode is converted by a large resistor to a voltage and then amplified by a homebuild circuit including a low noise operation amplifier. The whole MCP Chevron assembly is boxed into a Faraday cage in order to shield the atoms in the center of the chamber from the biased front side, typically charged with -2000 V. The Faraday cage is closed at the front by a grid with a diameter of 12 mm and a transmittance of 85%. The active area of the MCP front side has a diameter of 8.5 mm.

To detect the Rydberg atoms with an MCP one has at first to field ionize the excited atoms. This can be done by a large enough electric field, which is in the case of an $43S_{1/2}$ state about 160 V/cm. In our case we want to detect the ions and one has to provide besides a sufficient field strength also a suitable electric field distribution which guides the ions into the MCP J.

Usually the magnetic fields of the trapping potential are still switched on when the ions move towards the MCP. The combination of electric and magnetic fields provoke a drift on the ions according to the force $\vec{F} = q(\vec{E} + \vec{v} \times \vec{B})$. An estimation for the given experimental situation shows that the drift is in our case of the order of 1 mm and by this well below the aperture of the MCP of 8.5 mm.

We calibrated the MCP ion signal by monitoring the losses in a cold atomic cloud due to Rydberg excitation and the corresponding voltage signal on the anode. After amplification, which is the same for the subsequent experiments, we acquire a signal of 1 Vs per $3.65 \cdot 10^{10}$ atoms. In principle one could distinguish between single ion events, but the noise level of the signal limits our minimum sensitivity to about one hundred ions.

VII. RYDBERG EXCITATION OF MAGNETICALLY TRAPPED ATOMS

As a first performance test we excited Rydberg atoms in a magnetically trapped cloud of evaporatively cooled atoms. A schematic view of the experimental sequence is shown in Fig. 7. The ultracold cloud consisted of $4 \cdot 10^7$ atoms at a temperature of 15 μK confined in a cigar shaped harmonic trapping potential with an axial trapping frequency (along the z-axis) of 18 Hz and an radial trapping frequency of 310 Hz. The magnetic offset field at the center of the trapping potential was set to 1.0 Gauss and the cloud is spin polarized in the $F = 2, m_F = 2$

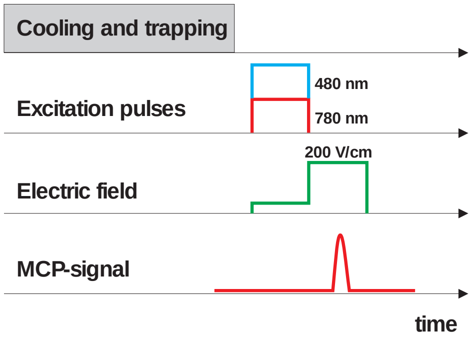

FIG. 7 Experimental sequence of Rydberg excitation. After the cooling and trapping steps are both lasers for the two photon excitation switched on simultaneously. The pulses can be as short as 200 ns. During laser excitation we apply an electric field over the atoms to induce a Stark shift. It is advantageous to apply a small electrical field also in other experiments to extract unwanted ions from the atomic cloud. To detect the generated Rydberg atoms we increase the electric field above 200 V/cm to field ionize them. After a short time of flight (few µs) the ions arrive at the MCP and generate after amplification a pulse on the anode which is recorded by a computer for further processing.

ground state with respect to the quantization axis given by the magnetic field. For highly excited states the hyperfine coupling is significantly decreased and we remain with the coupling of the electron spin to the orbital momentum to a total momentum J as shown in figure 8. We want to excite the atoms into the $43S_{1/2}$ state which exhibits the same magnetic moment as the ground state and the transition is insensitive to magnetic fields. The laser light of both beams is circular polarized (σ^+ for 780 nm and σ^- for 480 nm) with respect to the z-axis (bold arrows in Fig. 8). Nevertheless alters the direction of the magnetic field lines of a magnetic trapping potential when moving away from the center, which leads to a space dependent angle between the k-vector of the excitation lasers and the quantization axis. By this it is also possible to excite atoms into other excited states by admixtures of other polarizations.

Fig. 8 shows the measurement of an excitation spectrum. To avoid a too large excited state fraction and with this unwanted Rydberg-Rydberg interactions effects, we reduced the excitation time to 1 µs. During the excitation pulse we applied a small electric field of 2 V/cm to extract accidental ions. After excitation we immediately field ionized the Rydberg atoms and detected the ions with the multichannel-plate as described in section VI.

In an additional experiment, we measured the radiative lifetime of the $43S_{1/2}$ state at a temperature of 20 µK and a atomic peak density of $5 \cdot 10^{12}$ cm^{-3}. We measured a lifetime of 99±15 µs, which is nicely in accordance with the expected lifetime of 99 µs. The theoretical value has been calculated with the help of the quantum defects of ^{87}Rb (Gallagher, 1994). This shows that the lifetime is not reduced by collisions at such high

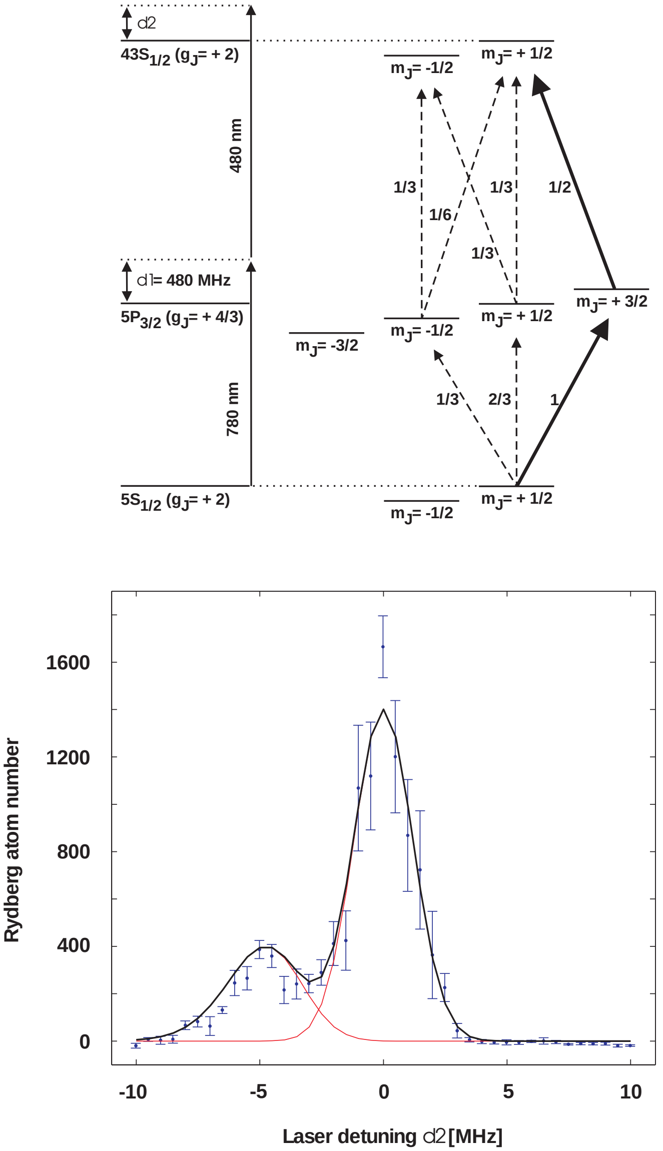

FIG. 8 Excitation of Rydberg atoms into the $43S_{1/2}$ state from a cloud of magnetically trapped atoms with a temperature of 15 μK. The upper part of the figure shows the two photon excitation scheme and the different pathways into the Rydberg states in the presence of a magnetic field as described in the text. The numbers next to the arrows indicate the individual transitions strengths. The measurement of the Rydberg excitation spectrum shown below features as expected two distinct peaks. The peak on the right corresponds to the in first order magnetically independent transition $5S_{1/2}, m_J = 1/2 \rightarrow\ 43S_{1/2}, m_J = 1/2$. The underlying red line is a Gaussian fit to the data with a width of 1.5 MHz. The peak on the left raises by the excitation into the $43S_{1/2}, m_J = -1/2$ state, which is sensitive to the magnetic field. The position and the shape of this peak is determined by the magnetic field distribution across the atomic cloud, the corresponding polarization pattern seen by the atoms, the temperature of the cloud, the excitation line-width and the different possible excitation paths. This has been calculated for the given parameters and the only remaining fitting parameter of the red curve is the height. Finally, the black curve is the sum of the two individual red fitting curves.

densities. One would expect a reduction of the lifetime by a factor of two due to blackbody radiation at 300 K (Gallagher, 1994), which is not seen in our experiment. This is most likely due to the strongly reduced spectral density of modes inside the metallic vacuum chamber (Kolokolov and Skrotskii, 1974).

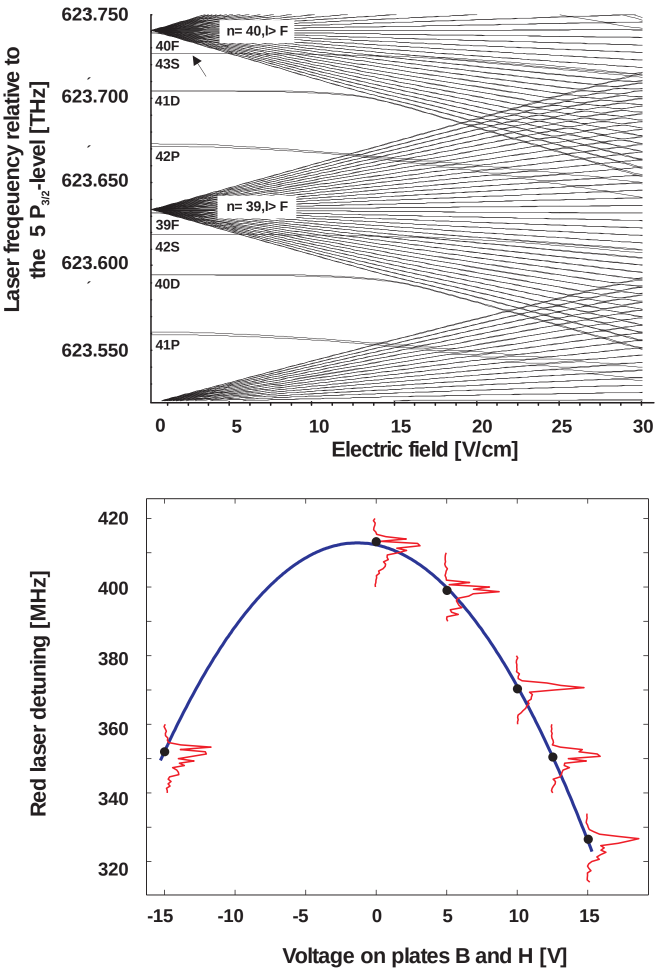

FIG. 9 The upper graph shows a theoretical calculation of the Stark shift in the vicinity of $n = 40$. The arrow indicates the Stark shift of the 43S state which we used in our measurements shown in the graph below. The solid blue line is a parabolic fit since a quadratic Stark shift is expected. The red curves show the corresponding ion signal detected on the MCPs. The center of masses are represented by the black dots.

VIII. ELECTRIC FIELD CALIBRATION BY MEASURING THE STARK SHIFT OF THE 43S$_{1/2}$ STATE

To examine the electric fields generated by the field plates, we make use of the quadratic Stark effect exhibited by the 43S$_{1/2}$ state. The energy shift ΔW (in units of Plancks constant) of this state located in an electric field E is given by

$$\Delta W = -\frac{1}{2}\alpha E^2 \tag{1}$$

with $\alpha/2 = 8.06\ \mathrm{MHz}/(\mathrm{V/cm})^2$. This value has been calculated by a first principles calculation of the Stark map as shown in Fig. 9.

The electric field for the Stark shift was produced by voltages on the field plates B and H, which were tuned from -15 V to +15 V. All other field plates as well the cage of the MCP I were set to ground. The simulation of the emerging field gives in the geometric center a value of 0.14 V/cm per applied unit of voltage on field plate B and H. The orientation of the field is parallel to the x-axis. The intrinsic asymmetric configuration of the field exhibits additionally a gradient along the x-axis of 0.1 V/cm^2 per applied unit volt. This field is superposed with an additional extraction field of the Faraday cage of the MCP J, which was charged to -15 V. The calculated field remaining from the cage at the center is 0.2 V/cm plus a gradient of 2 V/cm^2. For detection of the Rydberg atoms we switch after excitation the voltage on plate B and H to +1000 V, which is sufficient for field ionization. The field configuration with the plates B and H at a positive voltage and the Faraday cage at -15 V drags the positive ions towards the MCP for detection.

As a sample for excitation we used an evaporatively cooled atomic cloud confined in the magnetic trap. At a temperature of 40 µK the cloud is in the harmonic regime of the magnetic trap with a radial width of about 40 µm. For such small clouds one can neglect the broadening of the spectroscopic lines due to inhomogeneties of the electric field. For the given parameters above, the broadening is less than two percent of the magnitude of the Stark shift energy.

Fig. 9 shows the result on the measured Stark shift. The parabolic fit (blue line) is shifted by 1.34 V with respect to 0 V, which is caused by the additional offset field of the Faraday cage. At 0 V one gets a Stark shift of 0.58 MHz which corresponds to an offset field of 0.27 V/cm (calculated 0.2 V/cm). The curvature of the fitted parabola can be used to calibrate the electric field for the applied voltages at field plate B and H. To achieve 1 V/cm at the position of the atoms one has to apply 5 V at both field plates. The expected value from the theoretical calculation is 7.2 V. Both deviations from the theoretical can be explained if the atomic cloud is shifted along the x-axis by a few millimeters away from the geometric center. More likely are imprecisions of the numerical calculations, since the parametrization of the full vacuum chamber geometry is not feasible.

The spectroscopic lines (plotted in red) exhibit a broadening which is not independent of the applied electric field. There are two possible paths for the two photon transition $5S_{1/2} \rightarrow 5P_{3/2} \rightarrow 43S_{1/2}$. The desired transition ends in the $j = +1/2$ state of the $43S_{1/2}$ manifold, which is the only one allowed by the chosen polarizations.

Nevertheless, is the direction of the magnetic field adjacent to the trapping center not parallel to the z-axis and atoms can also be transferred to the $j = -1/2$ which is not anymore insensitive to the magnetic field. The g_j factor of the Rydberg state is 2 and the total change in magnetic momentum is 2 μ_B. A calculation for the given parameters results in a broadening of about 3 MHz, which explains the observed linewidths very well.

IX. CONCLUSION

In this article, we have presented details of designing a setup which combines quantum degenerate gases with Rydberg atoms. The capability of coherent excitation into specific Rydberg states and their efficient detection with multichannel-plates establishes a new framework to study coherence properties of mesoscopic quantum systems. Especially the tunability of the interaction strength and type among the Rydberg atoms by either choosing a specific Rydberg state or by applying electric fields make this a valuable system for many tasks. The first realization of coherent and collective excitation in a mesoscopic quantum system in the strong coupling regime has been achieved with this setup (Heidemann *et al.*, 2007). There exist manifold options for further investigations. This could be studies on the coherence properties of nonclassical states, the dependence on system size and its geometry, signatures beyond mean-field theories and the feasibility of such systems for quantum information.

X. ACKNOWLEDGMENTS

Funding of this setup was provided by the Deutsche Physikalischen Gesellschaft in the Schwerpunktprogramm (SPPP 1116) and by the Sonderforschungsbereich SFB/TR 21. The Rydberg laser system was partly funded by the Landesstiftung Baden-Württemberg. The authors thank Jörg Bauer, Christian Kuke, Johannes Nold, Eva Kuhnle and Helmar Bender for their contributions in setting up this experiment.

References

Afrousheh, K., P. Bohlouli-Zanjani, D. Vagale, A. Mugford, M. Fedorov, and J. D. Martin, 2004, Physical Review Letters **93**(23), 233001.

Amthor, T., M. Reetz-Lamour, S. Westermann, J. Denskat, and M. Weidemüller, 2007, Physical Review Letters **98**(2), 023004.

Anderson, W. R., J. R. Veale, and T. F. Gallagher, 1998, Physical Review Letters **80**, 249.

Bohlouli-Zanjani, P., K. Afrousheh, and J. D. D. Martin, 2006, Review of Scientific Instruments **77**, 3105.

Carroll, T. J., K. Claringbould, A. Goodsell, M. J. Lim, and M. W. Noel, 2004, Physical Review Letters **93**(15), 153001.

Chikkatur, A. P., Y. Shin, A. E. Leanhardt, D. Kielpinski, E. Tsikata, T. L. Gustavson, D. E. Pritchard, and W. Ketterle, 2002, Science (296), 2193.

Chu, S., 1998, Rev. Mod. Phys. **70**, 685.

Cohen-Tannoudji, C. N., 1998, Rev. Mod. Phys. **70**, 707.

Cornell, E. A., and C. E. Wieman, 2002, Rev. Mod. Phys. (74), 875.

Cubel, T., B. K. Teo, V. S. Malinovsky, J. R. Guest, A. Reinhard, B. Knuffman, P. R. Berman, and G. Raithel, 2005, Phys. Rev. A **72**(2), 023405.

Deiglmayr, J., M. Reetz-Lamour, T. Amthor, S. Westermann, A. L. de Oliveira, and M. Weidemüller, 2006, Optics Communications **264**, 293.

Demtröder, W., 2002, *Laser Spectroscopy* (Springer Verlag), 2nd edition.

DiVincenzo, D. P., 2000, Fortschr. Phys. **48**, 771.

Ernst, U., A. Marte, F. Schreck, J. Schuster, and G. Rempe, 1998, Euro. Phys. Lett. **41**, 1.

Farooqi, S. M., D. Tong, S. Krishnan, J. Stanojevic, Y. P. Zhang, J. R. Ensher, A. S. Estrin, C. Boisseau, R. Côté, E. E. Eyler, and P. L. Gould, 2003, Physical Review Letters **91**(18), 183002.

Fortagh, J., A. Grossmann, C. Zimmermann, and T. W. Hänsch, 1998, Phys. Rev. Lett. **81**(24), 5310.

Gallagher, T. F., 1994, *Rydberg Atoms* (Cambridge University Press).

Gupta, S., K. W. Murch, K. L. Moore, T. P. Purdy, and D. M. Stamper-Kurn, 2005, Physical Review Letters **95**(14), 143201 (pages 4).

Hänsel, W., P. Hommelhoff, T. Hänsch, and J. Reichel, 2001, Nature (498), 498.

Heidemann, R., U. Raitzsch, V. Bendkowsky, B. Butscher, R. Löw, L. Santos, and T. Pfau, 2007, ArXiv Quantum Physics e-prints eprint quant-ph/0701120.

Jaksch, D., J. I. Cirac, P. Zoller, S. L. Rolston, R. Cote, and M. D. Lukin, 2000, Phys. Rev. Lett. **85**, 2208.

Ketterle, W., 2002, Rev. Mod. Phys. (74), 1131.

Killian, T. C., S. Kulin, S. D. Bergeson, L. A. Orozco, C. Orzel, and S. L. Rolston, 1999, Phys. Rev. Lett. **83**(23), 4776.

Koch, P., 1983, *Rydberg studies using fast beams*, Rydberg states of atoms and molecules (Cambridge University Press).

Kolokolov, A., and G. Skrotskii, 1974, Opt. Spectrosc. **36**, 127.

Lett, P., W. D. Phillips, S. L. Rolston, C. E. Tanner, R. N. Watts, and C. I. Westbrook, 1989, J. Opt. Soc. Am. B **6**(11), 2084.

MacAdam, K. B., and C. S. Hwang, 2003, Review of Scientific Instruments **74**, 2267.

Mourachko, I., D. Comparat, F. de Tomasi, A. Fioretti, P. Nosbaum, V. M. Akulin, and P. Pillet, 1998, Physical Review Letters **80**, 253.

Ottl, A., S. Ritter, M. Kohl, and T. Esslinger, 2006, Review of Scientific Instruments **77**(6), 063118 (pages 18).

Phillips, W. D., 1998, Rev. Mod. Phys. **70**, 721.

Pritchard, D. E., 1983, Phys. Rev. Lett. **51**(15), 1336.

Robert, A., O. Sirjean, A. Browaeys, J. Poupard, S. Nowak, D. Boiron, C. I. Westbrook, and A. Aspect, 2001, Science (292), 5516.

Robinson, M. P., B. L. Tolra, M. W. Noel, T. F. Gallagher, and P. Pillet, 2000, Physical Review Letters **85**, 4466.

Singer, K., M. Reetz-Lamour, T. Amthor, L. G. Marcassa, and M. Weidemüller, 2004a, Physical Review Letters

93(16), 163001.

Singer, K., M. Reetz-Lamour, T. Amthor, L. G. Marcassa, and M. Weidemüller, 2004b, Physical Review Letters **93**(16), 163001.

Streed, E. W., A. P. Chikkatur, T. L. Gustavson, M. Boyd, Y. Torii, D. Schneble, G. K. Campbell, D. E. Pritchard, and W. Ketterle, 2006, Review of Scientific Instruments **77**(2), 023106 (pages 13).

Tong, D., S. M. Farooqi, J. Stanojevic, S. Krishnan, Y. P. Zhang, R. Côté, E. E. Eyler, and P. L. Gould, 2004, Physical Review Letters **93**(6), 063001.

Vogt, T., M. Viteau, J. Zhao, A. Chotia, D. Comparat, and P. Pillet, 2006, Physical Review Letters **97**(8), 083003.